DFT Description of the Magnetic Properties and Electron Localization in Dinuclear Di-μ-oxo-Bridged Manganese Complexes

Vincenzo Barone,[a] Alessandro Bencini,*[b] Dante Gatteschi,[b] and Federico Totti[b]

Abstract: Density functional theory (DFT) was applied to describe the magnetic and electron-transfer properties of dinuclear systems containing the $[MnO_2Mn]^{n+}$ core, with $n = 0,1,2,3,4$. The calculation of the potential energy surfaces (PESs) of the mixed-valence species ($n = 1,3$) allowed the classification of these systems according to the extent of valence localization as Class II compounds, in the Robin – Day classification scheme. The fundamental frequencies corresponding to the asymmetric breathing vibration were also computed.

Keywords: density functional calculations · electron transfer · magnetic properties · manganese · mixed-valent compounds

Introduction

Mixed-valence transition metal complexes are an important class of compounds since they show a number of peculiar physicochemical properties of relevance in different fields of science including chemistry, biology, and physics. Mixed-valence species can be regarded as formed by two or more transition metal centers bearing fractional formal charges, or, better, by integer valence-localized centers and "extra" electron(s) which can hop from one center to the other. When the metal centers have magnetic ground states, the interplay between electron delocalization and magnetic interactions plays a crucial role in determining their magnetic behavior, which is of current interest, for instance, in solid-state chemistry (bulk magnets and superconductors[1, 2]), inorganic chemistry (mixed-valence clusters and heteropolyblues[3]) and biology (iron – sulfur proteins[4, 5]).

The simplest mixed-valence systems are dinuclear complexes. They are simple enough to allow a very accurate experimental characterization of their physicochemical properties, and at the same time the use of the most sophisticated quantum-mechanical models to describe their electronic structure. Since the hopping electron retains its spin orientation during the transfer, in homonuclear transition metal dimers with more than one unpaired electron per metal site the spin state with the maximum spin multiplicity is always stabilized. This spin-dependent electron delocalization has been traditionally indicated with the term *double-exchange*.[6–8] The magnetic properties of dinuclear mixed-valence compounds are commonly rationalized through the use of a phenomenological spin Hamiltonian, which includes a super-exchange isotropic interaction between localized spin and an electron delocalization parameterized term.[9] A possible form of the double-exchange spin Hamiltonian is given by Equation (1), where the * indicates the atomic center onto which the "extra" electron with $s_e = 1/2$ is localized and $\boldsymbol{S}_k^* = \boldsymbol{S}_k + \boldsymbol{s}_e$.

$$H = J(\boldsymbol{S}_A^* \cdot \boldsymbol{S}_B + \boldsymbol{S}_A \cdot \boldsymbol{S}_B^*) + B\boldsymbol{T}_{AB} \quad (1)$$

The $B\boldsymbol{T}_{AB}$ term splits the localized states, $|S_A^* S_B S M_s\rangle$ and $|\boldsymbol{S}_A \boldsymbol{S}_B^* S M_s\rangle$, ($\boldsymbol{S} = \boldsymbol{S}_A^* + \boldsymbol{S}_B = \boldsymbol{S}_A + \boldsymbol{S}_B^*$) according to Equation 2 with $B = \dfrac{\beta}{2S_0 + 1}$.

$$\begin{aligned} T_{AB}|\ S_A^* S_B S M_s\rangle &= (S + 1/2)\,|S_A S_B^* S M_s\rangle \\ T_{AB}|\, S_A S_B^* S M_s\rangle &= (S + 1/2)\,|S_A^* S_B S M_s\rangle \end{aligned} \quad (2)$$

β(or t_{ab}, or H_{ab}) is the effective electron transfer integral between the magnetic orbitals occupied by the "extra" electron[10, 11] and S_0 is the spin of centers A and B (in the absence of the "extra" electron). The energy of the states with total spin S, $E(S)$, takes the form given in Equation 3, where a positive J value means an antiferromagnetic exchange interaction.

$$E_{\pm}(S) = J/2[S(S + 1)] \pm B(S + 1/2) \quad (3)$$

As mentioned above, the double-exchange parameter B always stabilizes the spin state with maximum spin, $S = S_{max} = S_A^* + S_B$. Depending on the B/J ratio, the S_{max} state can be the

[a] Prof. V. Barone
Dipartimento di Chimica
Università di Napoli "Federico II", Napoli (Italy)

[b] Prof. A. Bencini, Prof. D. Gatteschi, Dr. F. Totti
Dipartimento di Chimica, Via della Lastruccia, 3
Università di Firenze, Firenze (Italy)
Fax: (+39) 055 4573372
E-mail: alessandro.bencini@unifi.it

  0947-6539/02/0821-5019 $ 20.00+.50/0

ground state even overcoming an antiferromagnetic exchange interaction which stabilizes the $S_{min} = |S_A^* - S_B| = |S_A - S_B^*|$ state. The double-exchange interaction doubles the number of spin levels which correspond to the two linear combinations, $E_{\pm}(S)$, of the localized spin eigenfunctions. In the most favorable cases, transitions between $E_+(S)$ and $E_-(S)$ can be observed in the electronic absorption spectrum allowing the direct measurement of B. This transition is often indicated as E_{op}. It must be stressed at this point that the measurement of the temperature dependence of the magnetic susceptibility alone does not permit (in most of the cases experimentally encountered) the independent estimate of J and B, since, the susceptibility depends only on the low-lying thermally populated excited states, which share the same symmetry (+ or −) when $B > J$: therefore J and B are often strongly correlated.

The magnetic properties of mixed-valence dimers result from the interplay of double- and super-exchange interactions. In actual compounds double-exchange interactions are modulated by trapping effects which, reducing the double-exchange effect, lead sometimes to an antiferromagnetic ground state. These trapping effects can be static, that is caused by chemical differences in the A and B sites, or dynamic, that is caused by vibronic interactions. In a widely used classification scheme,[12] mixed-valence systems are divided into three classes depending on the amount of delocalization of the "extra" electron: in Class III compounds the "extra" electron is completely delocalized and in Class I systems it is completely localized on one of the metal ions. Class II compounds have an intermediate behavior, which often leads to a temperature-dependent degree of localization.

The theoretical characterization of mixed-valence compounds requires a computational approach which is able to model super- and double-exchange interactions including the dependence of the electron localization on the nuclear displacements. Recently, we have applied density functional theory (DFT) to characterize the electronic properties of two Class III mixed-valence complexes, namely the Creutz–Taube cation[13] and the $[Fe_2(OH)_3(tmtacn)_2]^{2+}$ complex (tmtacn = *N*,*N*′,*N*″-trimethyl-1,4,7-triazacyclonorane)[14] and we developed a computational approach for the characterization of mixed-valence transition metal dimers which includes a vibronic analysis of the potential energy surface (PES) of the ground and lowest excited states of the systems. To further investigate the reliability of our approach, we decided to compute the electronic structure of doubly, oxygen-bridged pseudo-octahedral Mn^{III}/Mn^{IV} dimers, since a number of complexes of general formula $[MnO(L_4)]_2^{3+}$ (L_4 = nitrogen ligand) have been synthesized in the last few years[15, 16] to mimic the active site of biologically important metalloenzymes,[17] and have been experimentally assigned to Class II. No analogous Mn^{II}/Mn^{III} systems of the formula $[MnO(L_4)]_2^{+}$ have been reported so far. Recently a Class II Mn^{II}/Mn^{III} couple was reported with Mn in a tetrahedral coordination.[18] To include a full characterization of the magnetic interactions in dimanganese systems we have computed the electronic and magnetic structures of the integer valence systems, $[MnO(L_4)]_2^{0/2+/4+}$, covering the whole range of stable oxidation states, and completing the calculation already performed by other groups.[19, 20] Also in this case, complexes with zero charge, formally formed by Mn^{II} ions, have not yet been synthesized. In all the known complexes with formula $[MnO(L_4)]_2^{2+/4+}$ the manganese ions were found to be antiferromagnetically coupled; the J values ranged from 170 to 300 cm^{-1} according to the nature of the L_4 ligand and to the oxidation state.[16a–d, 21]

To eliminate the dependence of the computed properties on the specific nature of the terminal ligand, we used the model complex $[Mn_2O_2(NH_3)_8]^{n+}$ (Figure 1) in all the calculations.

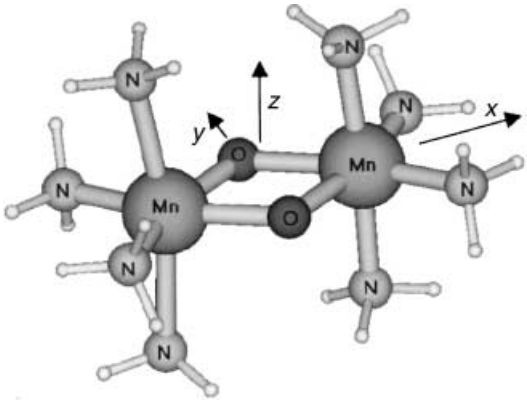

Figure 1. Schematic structure of the model complex $[Mn_2O_2(NH_3)_8]^{n+}$ (n = 0–4) used in the DFT calculations.

Following previous studies,[14, 20] the four nitrogen atoms of the ligands were replaced by ammonia molecules. It has to be stressed here that the replacement of the real ligands by simpler molecules can affect the computed J values in a significant way, so that a quantitative comparison with the experimental values can be questionable; on the other hand relative variations of the magnetic parameters and magneto-structural correlations can always be extracted.[22] A striking example is provided by the $[(tert\text{-butpy})_2Cu(N_3)_2Cu(tert\text{-butpy})]^{2+}$ (*tert*-butpy = *tert*-butylpyridine) compound: a coupling constant in good agreement with experimental data could be computed only using pyridine as ligand, whereas the ammonia model leads to incorrect results almost irrespective of the computational level.[22] It is also known that inclusion of some HF exchange in the functional (B3LYP functional,[23] for instance), stabilizes the high-spin states and, in general, improves the agreement with the experimental data. The results are, however, strongly dependent on the ratio (ρ) between HF and local exchange,[22, 24] and optimized values of ρ are not yet available for magnetic properties. As a consequence we will use only conventional density functionals here.

Computational Details

DFT calculations were performed with the Amsterdam Density Functional (ADF) program package, version 2.3.[25, 26] The standard basis sets provided within the package were used throughout. Double-ζ STO basis sets were employed to describe the valence orbitals of all non-hydrogen atoms, except the manganese 3d orbitals which were represented by using a triple-ζ function. The shells up to 2p for Mn and 1s for all the other non-hydrogen atoms were treated as frozen cores. Single-ζ STO basis sets were used for hydrogen atoms. An overall C_{2v} symmetry, which is a subgroup of the

0947-6539/02/0821-5020 $ 20.00+.50/0 *Chem. Eur. J.* **2002**, *8*, No. 21

highest D_{2h} molecular symmetry, was used in the calculations, if not otherwise specified.

The Xα functional[27] was used for the exchange and Vosko, Wilk, and Nusair functionals[28] for the correlation potential (LSDA approximation). The Stoll's dynamical correlation correction[29] was also applied in all the calculations. Anharmonic frequencies needed for the estimation of vibronic couplings (vide infra) were computed by the DiNa package.[30]

The calculation of the exchange-coupling constant, J, involved the determination of the energies of the spin multiplets of the dimer. This task cannot be accomplished within a single determinant formalism like DFT, and some approximate procedure must be used.[31] A widely used formalism, the broken symmetry approach,[32] is based, for weakly interacting magnetic ions, on a one-to-one mapping of the exact Hamiltonian over the spin Hamiltonian. This mapping is performed by equating the energy of an appropriate single determinant issuing from an SCF computation to the energy of its counterpart on a product spin basis $\{_i \mid S_i M_{S_i}\}$ expressed as a function of the spin Hamilitonian parameter J. The highest spin state (that is the ferromagnetic one), is usually approximated by a single Slater determinant, allowing the density functional to account for the short-range or dynamic correlation effects. The energy of this determinant, which is also an eigenstate of S^2 to a good approximation, is compared with the matrix element of the highest spin eigenfunction, $\Pi_i \mid S_i M_{S_i}\rangle$, computed with the isotropic spin Hamiltonian. The lowest spin state (that is the antiferromagnetic one), is approximated by a determinant built with molecular orbitals localized on the different spin centers of the clusters bearing each center in its internal high spin state, but with overall spins opposed to each other: the broken symmetry state. This determinant is in general an eigenfunction of S_z only. The orbitals obtained through this procedure originate from a spin-unrestricted SCF calculation, and are localized with a non-orthogonal spatial part. Therefore they can be identified with the natural magnetic orbitals of the system.[9] The energy of the broken symmetry determinant is compared with the matrix element of the spin Hamiltonian in the basis $\{\Pi_{i+j}(\mid S_i M_{S_i}\rangle \mid S_i - M_{S_i}\rangle)\}$. For dinuclear systems this procedure yields the general expression given in Equation 4 for J, where S_{max} stays for the highest spin state of the system.

$$J = \frac{E(S_{max}) - E(S_{BS})}{2S_A S_B} \quad (4)$$

Since Equation (4) holds only for weakly interacting magnetic systems, that is when the squared overlap between the magnetic orbitals is much lower than 1, J values computed in this way provide an upper limit of the exchange-coupling constant. In the opposite situation, when a strong bonding interaction occurs, the energy of the broken symmetry state is close to the energy of the lowest energy multiplet, as discussed at some length in the recent literature.[22, 31, 33, 34] Since the computed magnetic orbitals (vide infra) are rather well localized on the two manganese centers in the integer valence systems, we will use Equation (4) to compute the J values.

The procedure for the calculation of the spin Hamiltonian parameters for the mixed-valence complexes[32e] will be briefly explained in the text.

Geometry optimizations were performed by using the Broyden–Fletcher–Goldfarb–Shanno hessian update and default criteria of convergence on energy, cartesians, and gradient were applied. Optimizations were always performed on the high-spin state since it can be meaningfully described using a single Slater determinant. We prefer this approach to the use of the broken symmetry wavefunction which in general does not represent any pure spin state.

Table 1. Comparison between computed relevant geometrical parameters for the $[Mn_2O_2]^{n+}$, $n = 0, 2, 4$, and the available experimental data.[a]

	Mn^{II}/Mn^{II}	Mn^{III}/Mn^{III} [b,c]	Mn^{IV}/Mn^{IV} [b,d]
Mn–Mn	2.656	2.703 (2.674–2.686)	2.780 (2.672–2.748)
Mn–O	1.975	1.851 (1.830–1.842)	1.845 (1.774–1.811)
Mn–N_{ax}	2.329	2.337 (2.323–2.427)	2.046 (2.007–2.010)
Mn–N_{eq}	2.357	2.119 (2.098–2.123)	2.099 (2.060–2.076)
O-Mn-O	96.7	86.2 (86.1–86.7)	82.3 (78.5–85.0)

[a] Distances in Å, bond angles in °. [b] Experimental data in parenthesis. The observed range of values are reported. Structural data for Mn^{III}/Mn^{III}(bispicen)$_2$,[16a,q] Mn_2^{III}/Mn^{III}(bispyzen)$_2$,[16a] Mn_2^{III}/Mn^{III}(6-Me_2tmpa)$_2$,[16a] Mn_2^{IV}/Mn^{IV}(bispicen)$_2$,[16b] Mn_2^{IV}/Mn^{IV}(phen)$_2$,[16c] Mn_2^{IV}/Mn^{IV}(6-MeL_1)$_2$.[16d] Ligands: bispicen = *N*,*N*′-bis(2-pyridylmethyl)-1,2-ethanediamine, bispyzen = *N*,*N*′-bis(pyrazin-2-ylmethyl)ethane-1,2-diamine, 6-Me_2-tmpa = *N*,*N*-bis[(6-methylpyridin-2-yl)methyl]-*N*-(pyridin-2-ylmethyl)amine, phen = 1,10-phenanthroline, 6-MeL_1 = *N*-[(6-methylpyridin-2-yl)-methyl]-*N*,*N*-bis(pyridin-2-ylmethyl)amine. [c] The values computed on the broken symmetry state using the Becke–Perdew functional[20] are: Mn–Mn 2.716 Å, Mn–O 1.840 Å, Mn–N_{ax} 2.504 Å, Mn–N_{ax} 2.231 Å, O-Mn-O 84.8°. [d] The optimized values on broken symmetry using the Becke–Perdew functional[20] are, respectively: Mn–Mn 2.866 Å, Mn–O 1.842 Å, Mn–N_{ax} 2.137 Å, Mn–N_{ax} 2.215 Å, Mn-O-Mn 77.9°.

Table 2. Comparison between computed relevant geometrical parameters for the $[Mn_2O_2]^{n+}$, $n = 1,3$ and the available experimental data.[a]

	Mn_2^{II}/Mn^{III}		Mn_2^{III}/Mn^{IV} [b,c]	
	C_{2v}	D_{2h} [d]	C_{2v}	D_{2h} [d]
Mn–Mn	2.693	–	2.746 (2.643–2.741)	–
Mn^{II}–O	2.015	1.930	–	–
Mn^{III}–O	1.822	1.930	1.907 (1.814–1.862)	1.850
Mn^{IV}–O	–	–	1.794 (1.774–1.827)	1.850
Mn^{II}–N_{ax}	2.281	2.322	–	–
Mn^{III}–N_{ax}	2.385	2.322	2.341 (2.128–2.349)	2.150
Mn^{IV}–N_{ax}	–	–	2.031 (2.013–2.220)	2.150
Mn^{II}–N_{eq}	2.348	2.265	–	–
Mn^{III}–N_{eq}	2.176	2.265	2.096 (2.079–2.132)	2.118
Mn^{IV}–N_{eq}	–	–	2.117 (2.053–2.128)	2.118
O-Mn^{II}-O	85.2	91.5	–	–
O-Mn^{III}-O	96.8	91.5	83.8 (80.6–84.0)	83.8
O-Mn^{IV}-O	–	–	96.8 (82.8–86.8)	83.8

[a] Distances in Å, bond angles in °. [b] Experimental data in parenthesis. The observed range of values are reported. Structural data for Mn^{III}/Mn^{IV}(6-MeL_1)$_2$,[16d,q] Mn^{III}/Mn^{IV}(bispicen)$_2$,[16e,q] Mn^{III}/Mn^{IV}(tren)$_2$,[16f] Mn^{III}/Mn^{IV}(bpy)$_2$,[16c,g,h,i] Mn^{III}/Mn^{IV}(phen)$_2$,[16c,g,h] Mn^{III}/Mn^{IV}(tmpa)$_2$,[16l,m] Mn^{III}/Mn^{IV}(cyclam)$_2$[16n,o] Mn^{III}/Mn^{IV}(pmap)$_2$.[16p] Ligands: 6-MeL_1 = *N*-[(6-methylpyridin-2-yl)methyl]-*N*,*N*-bis(pyridin-2-ylmethyl)amine, bispicen = *N*,*N*′-bis(2-pyridylmethyl)-1,2-ethanediamine, tren = tris(2-aminoethyl)-amine, bpy = 2,2′-pyridine, phen = 1,10-phenantroline, tmpa = tris(2-pyridylmethyl)amine, cyclam = 1,4,8,11-tetraazacyclotetradecane, pmap = bis[2-(2-pyridyl)ethyl]-2-pyridylmethylamine. [c] The values computed from optimizations on the broken symmetry state using the Becke–Perdew functional[20] are, respectively: Mn^{III}–Mn^{IV} 2.783 Å, Mn^{III}–O 1.873 Å, Mn^{IV}–O 1.800 Å, Mn–N_{ax} 2.459 Å, Mn^{IV}–N_{ax} 2.117 Å, Mn^{III}–N_{eq} 2.210 Å, Mn^{IV}–N_{eq} 2.227 Å, O-Mn^{III}-O 79.5°, O-Mn^{IV}-O 85.2°. [d] Optimization performed on a geometry constrained to D_{2h} symmetry, that is equivalent metal centers (see text).

Results and Discussion

Structural considerations: The geometrical structure of the model complexes was optimized for $[Mn_2O_2(NH_3)_8]$ (Mn^{II}/Mn^{II}, $S_{max} = 5$), $[Mn_2O_2(NH_3)_8]^{+}$ (Mn^{II}/Mn^{III}, $S_{max} = 9/2$), $[Mn_2O_2(NH_3)_8]^{2+}$ (Mn^{III}/Mn^{III}, $S_{max} = 4$), $[Mn_2O_2(NH_3)_8]^{3+}$ (Mn^{III}/Mn^{IV}, $S_{max} = 7/2$), $[Mn_2O_2(NH_3)_8]^{4+}$ (Mn^{IV}/Mn^{IV}, $S_{max} = 3$). The results of the calculations are summarized in Table 1 and Table 2 for the integer and the mixed-valence systems, respectively. In the same tables the available experimental data (Mn^{III}/Mn^{III}, Mn^{III}/Mn^{IV}, Mn^{IV}/Mn^{IV})[16] are also reported together with the results of previous calculations by Stranger and McGrady[20] on Mn^{III}/Mn^{III}, Mn^{III}/Mn^{IV}, Mn^{IV}/Mn^{IV} complexes. The optimizations were performed by using the broken symmetry wavefunction and the Becke–Perdew[35] gradient-corrected functional. A comparison between the two results shows that the Mn–Mn and Mn–N bond lengths

are generally overestimated in the latter approach and the broken symmetry geometries are in worse agreement with the experimental data.

A regular variation of some geometrical parameters is observed: on passing from Mn^{II}/Mn^{II} to Mn^{IV}/Mn^{IV} the Mn–Mn distance and the Mn-O-Mn angle increase. The Mn–O distances decrease in the Mn^{II}/Mn^{II}, Mn^{III}/Mn^{III}, and Mn^{IV}/Mn^{IV} cases and becomes quite different in the mixed-valence species. In the MnN_4 coordination polyhedron the axial Mn–N bond lengths are slightly shorter than the equatorial ones in Mn^{II}/Mn^{II} and Mn^{IV}/Mn^{IV}, and larger in Mn^{III}/Mn^{III}. The distortions may be due to the *trans* effect of the oxygen atoms (Mn^{II}/Mn^{II} and Mn^{IV}/Mn^{IV}) and to a static Jahn–Teller distorsion active in the Mn^{III} ion. The elongated coordination of Mn^{III} is, of course, present also in the Mn^{II}/Mn^{III} and Mn^{III}/Mn^{IV} systems. These computed geometries will be used in the following for the calculation of the static magnetic parameters.

Antiferromagnetism in the integer valence Mn^{II}/Mn^{II}, Mn^{III}/Mn^{III}, and Mn^{IV}/Mn^{IV} species: The values of the exchange coupling constant *J*, computed using Equation (4), are shown in the first-row of Table 3 and compared with the available experimental data. While our computations indicate that in all the compounds the Mn ions are antiferromagnetically coupled, as experimentally observed in the Mn^{III}/Mn^{III} and Mn^{IV}/Mn^{IV} cases, the calculated strength of the coupling is overestimated compared to the experiment. This overestimation of *J* is a common drawback of broken symmetry calculations, and has been already discussed.[22, 34, 36] This can be due to the assumption (implicit in deriving Equation (4)) of a weak bonding interaction between the magnetic centers, or to the modeling of the system, or to the combination of both effects. Applying the strong bonding approach, as is sometimes done in the literature,[37] the *J* values obtained for the complexes $[Mn_2O_2(NH_3)_8]^{2+}$ and $[Mn_2O_2(NH_3)_8]^{4+}$ were 382 and 524 cm^{-1}, respectively. Although these values are closer to the experimental data, a good quantitative agreement is still lacking: in our opinion, this is due to the actual modeling of the complexes which includes deviation from the real systems in the bonding nature of the terminal ligands and in some of the geometrical parameters. A similar overestimation of the *J* values was found also in reference [19], where GGA functionals were used. An estimate of the limit of validity of Equation (4) can be obtained by computing the average value of $\boldsymbol{S}^2$ on the broken symmetry state, $\langle \boldsymbol{S}^2 \rangle$. This value should be close to 0 (pure singlet state) when there is a strong overlap between magnetic orbitals, and to the number of β electrons occupying the magnetic orbitals when they are orthogonal. The computed values for Mn^{II}/Mn^{II}, Mn^{III}/Mn^{III}, and Mn^{IV}/Mn^{IV} are 4.8, 3.6, and 2.6, respectively, indicating that the weak bonding approximation is reasonable.

Table 3. *J* values[a] for $[Mn_2O_2]^{n+}$, $n = 0, 2, 4$.

	Mn^{II}/Mn^{II}	Mn^{III}/Mn^{III}	Mn^{IV}/Mn^{IV}
J	78	478 (172–201)[b]	697 (252–288)[c]
J_s[d]	–	344	548

[a] Values in cm^{-1}. [b] Experimental value in parenthesis. The observed value is reported in references[16a,q]. [c] Experimental value in parenthesis. See references [16b,c]. [d] Values computed in reference [19] properly transformed for the spin Hamiltonian of Equation (1).

In the DFT description of the magnetism of the molecule, quantitative relationships with individual exchange pathways are lost, since they are strictly related, in a molecular orbital model, to a configuration interaction development of the wavefunction.[9, 38] Qualitative considerations on the exchange pathways can be, however, derived by looking at the composition of the magnetic orbitals as obtained by the broken symmetry approach and already outlined in reference [20].

The computed *J* value decreases when the formal charge on manganese is reduced from +4 to +2. This behavior is due to two main factors: the variation of the composition of the magnetic orbitals and the geometrical changes, in particular the Mn-O-Mn angle, associated to the charge of the complexes. The magnetic orbitals of all the model complexes are shown in Figure 2.

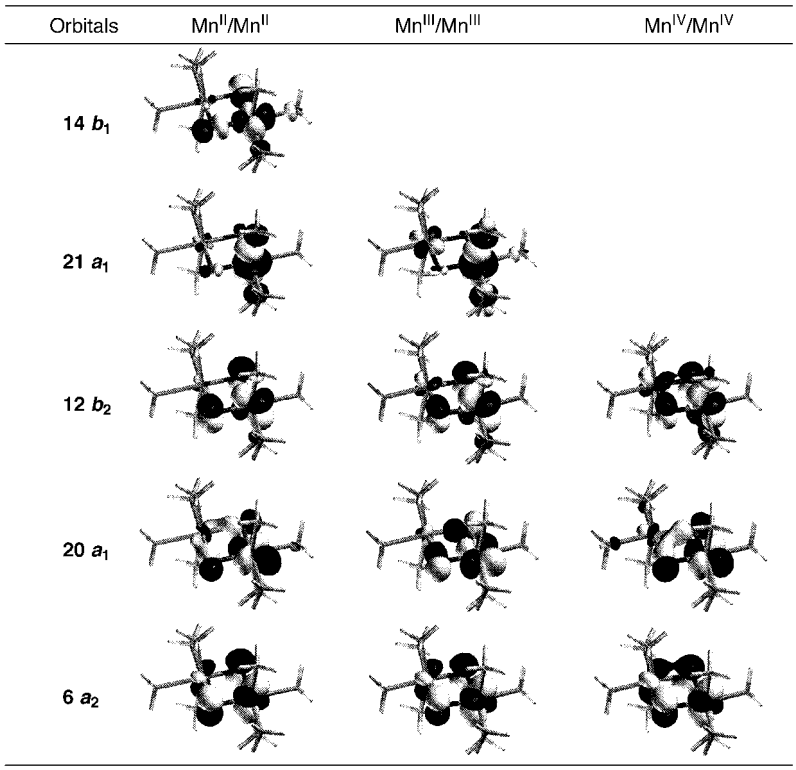

Figure 2. Isosurface representations of the magnetic orbitals for the complexes **1**, **3**, and **5**. The surfaces drawn correspond to $\psi = \pm 0.05$ au.

0947-6539/02/0821-5022 $ 20.00+.50/0 *Chem. Eur. J.* **2002**, *8*, No. 21

Mn^{IV}/Mn^{IV}: In the ground state each Mn^{IV} ion ($3d^3$) has all the t_{2g}-like (π^*) orbitals semioccupied (t_{2g}^3 configuration in a octahedral crystal field). These orbitals can be labeled in the C_{2v} point group symmetry as: $d_{x^2-y^2} \in a_1$, $d_{yz} \in a_2$, $d_{xz} \in b_2$. The empty e_g-like (σ^*) orbitals, d_{z^2} and d_{xy} span the a_1 and b_1 irreducible representations, respectively. The computed magnetic orbitals, shown in Figure 2, are mainly localized on one metal center, with a significant distribution of electron density onto the bridging oxygen atoms and on the other metal center. Only the α components are shown, the corresponding β components being isoenergetic and localized on the other half of the molecule. Larger delocalization generally means a better overlap between the α and β magnetic orbitals. In particular, the contribution of metal d orbital on the other center can be effective in transmitting the exchange interaction. We will call this contribution a "direct" interaction between the magnetic orbitals, which has to be added to the superexchange one which occurs through the electron delocalization onto the ligands. This direct interaction can lead to a, say α, electron delocalization on the other center onto the same orbital in which the, say β, electron is localized, or in an orbital which is orthogonal to it. In the first case a "direct" antiferromagnetic contribution can be expected, while a ferromagnetic interaction is expected in the latter case. The strength of the interaction will be roughly proportional to the transferred electron density.[39] Since both the $d_{x^2-y^2}$ and the d_{z^2} orbitals belong to the a_1 irreducible representation, they can be admixed, as is apparent from the composition of the $20a_1$ and $21a_1$ orbitals. According to the orbital models for the magnetic interaction,[9] three antiferro- and three ferromagnetic exchange pathways originate from the d^3-d^3 interaction, namely J_{a1a1}, J_{a2a2}, J_{b2b2}, and J_{a1a2}, J_{a2b2}, J_{a1b2}. Owing to the delocalization of the electron density on the bridging ligands, which favors the overlap between the magnetic orbitals and the antiferromagnetic interactions, the overall exchange coupling constant, $J = (J_{a1a1} + J_{a2a2} + J_{b2b2} + 2J_{a1a2} + 2J_{a2b2} + 2J_{a2b2})/9$, should be antiferromagnetic. The strength of the J_{ij} couplings is expected to be proportional to the square of the overlap integrals between the magnetic orbitals, which we report in Table 4 for Mn^{II}/Mn^{II}, Mn^{III}/Mn^{III}, and Mn^{IV}/Mn^{IV}. The leading term in Mn^{IV}/Mn^{IV} is the interaction between the d_{xz} orbitals which are mostly delocalized and efficiently overlap through the π interaction with the p_z orbitals of the bridging oxygens (Figure 2). Therefore, it can be expected that $J_{b2b2} \gg J_{a2a2} > J_{a1a1}$. $\langle b_2 \mid b_2 \rangle$ is smaller in the Mn^{III}/Mn^{III}, and Mn^{II}/Mn^{II} complexes. It can be seen from Figure 2 that on passing from Mn_2^{IV}/Mn^{IV} to Mn_2^{II}/Mn^{II} the "direct" contribution to the exchange interaction also decreases.

Table 4. Squared overlap integrals between the magnetic orbitals for the $[Mn^{(N)}{}_2O_2(NH_3)_8]^{n+}$ ($n = 0, 2, 4$; N = II, III, IV) cations.[a]

n/N	$\langle b_2 \mid b_2 \rangle^2$	$\langle a_2 \mid a_2 \rangle^2$	$\langle a_1 \mid a_1 \rangle^2$	$\langle a_1(z^2) \mid a_1(z^2) \rangle^2$	$\langle b_1 \mid b_1 \rangle^2$	$\langle a_1 \mid a_1(z^2) \rangle^2$
4/IV	0.96	0.058	0.019	–	–	–
2/III	0.015	0.046	0.0051	0.0034	–	0.097
0/II	0.024	0.0020	0.064	0.00	0.048	0.0039

[a] The magnetic orbitals are labeled according to the C_{2v} symmetry group (see text).

Mn^{III}/Mn^{III}: The two electrons added to the Mn^{IV}/Mn^{IV} dimer go in magnetic orbitals ($21a_1$) mainly localized on d_{z^2} orbitals on the two centers (see Figure 2). Therefore further exchange pathways are present which involve d_{z^2}: the d_{z^2}– d_{z^2} and the $d_{x^2-y^2} - d_{z^2}$. The computed overlap integrals, 0.0583 and 0.311, respectively, indicate that the first interaction should be weakly antiferro- or even ferromagnetic, while a significant antiferromagnetic coupling is expected from the $d_{x^2-y^2} - d_{z^2}$ interaction. Indeed, Figure 2 shows that the $21a_1\alpha$ magnetic orbital is significantly delocalized onto the $d_{x^2-y^2}$ orbital of the other Mn center onto which the $20a_1\beta$, magnetic orbital is localized. This "direct" mechanism thus favors a ferromagnetic $d_{z^2} - d_{z^2}$ interaction and a more sizable antiferromagnetic $d_{x^2-y^2} - d_{z^2}$ interaction. The other magnetic orbitals, mainly t_{2g}-like, closely resemble those computed for Mn^{IV}/Mn^{IV}, but the overlap integrals (Table 4) are smaller leading to a smaller antiferromagnetic effective interaction. A decrease in the overall J value is therefore expected.

Mn^{II}/Mn^{II}: The smallest J value ($J = 78\ cm^{-1}$) was computed for this system. The e_g-like orbitals are semioccupied and the number of ferromagnetic interactions increases, while the overlaps between the magnetic orbitals are comparable to or smaller than those computed for the Mn^{III}/Mn^{III} case (Table 4). The overall decrease of the overlap integrals on going from Mn^{IV}/Mn^{IV} to Mn^{II}/Mn^{II} follows the decrease of the Mn-O-Mn bridge from 97.7° in Mn^{IV}/Mn^{IV} to 83.9° in the actual case. A similar trend has been observed for the Mn–Mn distance which is reduced from 2.780 Å in Mn^{IV}/Mn^{IV} to 2.656 in the case under scrutiny.

Electron delocalization and antiferromagnetism in the mixed-valence Mn^{II}/Mn^{III} and Mn^{III}/Mn^{IV} species: The "extra" electron added to Mn^{III}/Mn^{III} to form the Mn^{II}/Mn^{III} species goes in one of the two possible linear combinations of the d_{xy} orbitals. The energy difference between the two configurations will be used later to compute the electron delocalization parameter. In a similar way the Mn^{III}/Mn^{IV} species is formed by adding the "extra" electron to the Mn^{IV}/Mn^{IV} in one of the MOs originating from the d_{z^2} atomic orbitals. Modeling of valence trapping effects requires the knowledge of the potential energy surface of the system as a function of the position of the atomic nuclei. In the simplest model of the valence trapping,[9] that is two uncoupled harmonic oscillators centered on the two Mn complexes, the localization of the "extra" electron is bound to the antisymmetrical breathing vibration, Q, which, for the Mn^{III}/Mn^{IV} case, is schematically represented in the Scheme 1.

The Mn^{III} center is in an axially elongated environment. The optimized geometrical parameters reported in Table 2 show that a similar scheme is also valid for the Mn^{II}/Mn^{III} case, albeit with a smaller distortion. In this picture, $Q = 0$ corresponds to the symmetrical situation (D_{2h} symmetry,

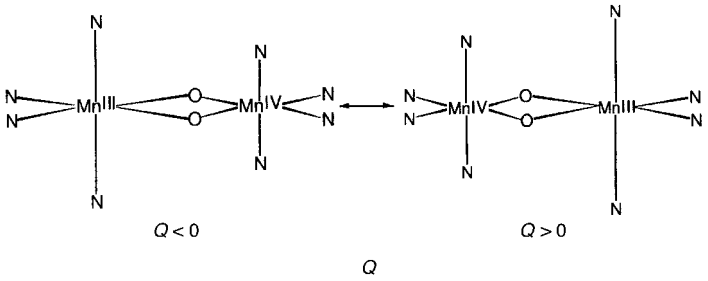

Scheme 1.

Table 2) located at higher energy. In previous papers[13, 14] we showed that the Q coordinate could be traced with good approximation by following the geometrical rearrangements of the molecules upon displacement of the bridging groups from the equilibrium geometry, computed with constrained geometrical optimizations. In the present case, geometry optimizations were performed on the Mn^{II}/Mn^{III} and Mn^{III}/Mn^{IV} systems with the Mn–Mn distance fixed at the optimized values (2.693 Å and 2.746 Å for Mn^{II}/Mn^{III} and Mn^{III}/Mn^{IV}, respectively) and displacing the O_2 moiety along the Mn–Mn (x axis) direction. All the other geometrical parameters were free of varying. This geometrical variation can be parameterized with the coordinate Q_O, computed as the distance between neighboring structures in mass-weighted coordinates. Of course, the structures issuing from the calculations must be properly oriented to eliminate spurious rotational components.[40] In this way we obtained an effective adiabatic potential energy curve (PEC). The calculations were performed on the high-spin states of the systems ($S = 9/2$ and $S = 7/2$ for Mn^{II}/Mn^{III} and Mn^{III}/Mn^{IV}, respectively). The computed PECs are plotted in Figure 3. It must be pointed out that, contrary to the simple model of Scheme 1, the maximum of the PEC at $Q_O = 0$ does not correspond to the symmetric structure (D_{2h}) but to a structure in which the Mn^{III} is weakly compressed. This can be understood by taking into consideration that an axial elongation (reminiscent of the Jahn–Teller effect) stabilizes the d_{z^2} orbital of Mn^{III} and, as a consequence, the whole system, and indicates that the Jahn–Teller stabilization can play a significant role in the electron delocalization mechanism. From this PEC, an effective one-dimensional Schrödinger equation can be derived,[41] whose numerical solution[30] provides the anharmonic frequencies associated to the motion along Q. All these steps are fully automated in the program package DiNa.[30] The vibrational eigenstates and frequencies computed by the above approach are shown in Figure 3. The motion is strongly anharmonic and the force constants corresponding to the harmonic component are $k_1 = 1409\ cm^{-1}\ Å^{-2}$, and $k_2 = 5618\ cm^{-1}\ Å^{-2}$ for the Mn^{II}/Mn^{III} and Mn^{III}/Mn^{IV} cases, respectively. From Figure 3 it is quite apparent that the minimum energy structure is significantly more distorted with respect to the delocalized arrangement for the Mn^{II}/Mn^{III} than for the Mn^{III}/Mn^{IV} system ($Q_{min}, \approx \pm 3$ and ± 1 amu$^{1/2}$bohr, respectively). At the same time, the activation energies governing the motion along Q_0 are comparable (≈ 600 and $\approx 800\ cm^{-1}$, respectively). The consequence of this behavior is that only the Mn^{III}/Mn^{IV} system shows a non negligible splitting between the first pair of symmetric and antisymmetric states (16 cm^{-1}).

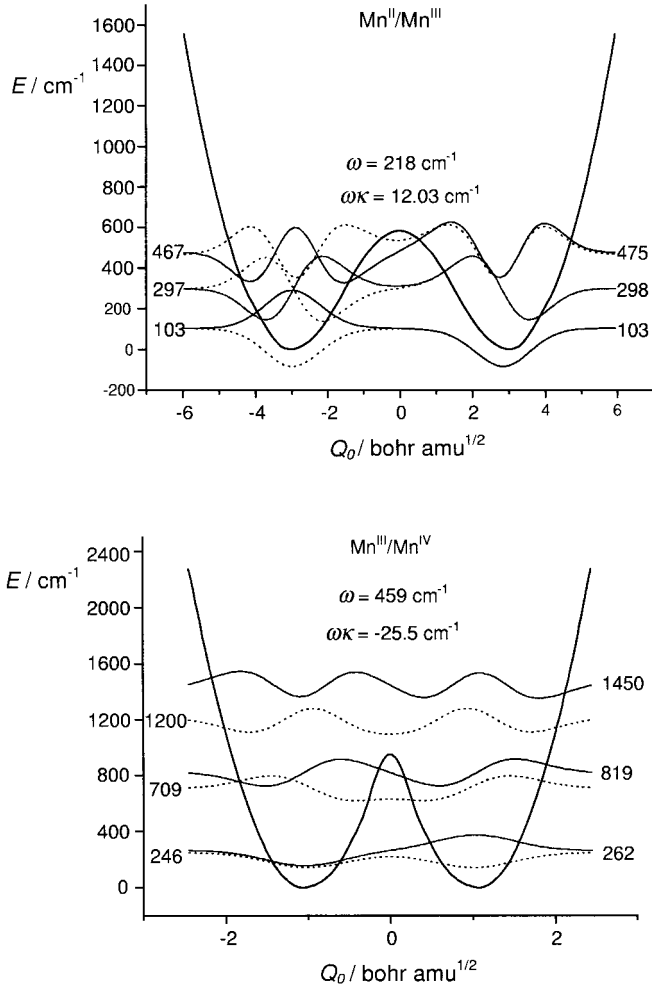

Figure 3. Computed potential energy curves for $[Mn_2O_2(NH_3)_8]^+$ (top) and $[Mn_2O_2(NH_3)_8]^{3+}$ (bottom). Vibrational eigenstates (left and right) and harmonic (ω) and aharmonic (ω_k) frequencies computed as described in the text are indicated.

Since the displacement of the ammonia molecules contributes significantly to the Q_O coordinate, particularly in the Mn^{III}/Mn^{IV} complex, we computed a two-dimensional potential energy surface (PES) including explicitly the variation of the distances of the ammonia ligands as a further degree of freedom. To this end we introduced the normal coordinate

$$q_N = \frac{q_N^{III} + q_N^{IV}}{\sqrt{2}}$$ where the local coordinates q_N^i

are given by Equation (5).

$$q_N^i = \frac{2\Delta R_{ax}^i - \Delta R_{eq}^i}{\sqrt{3}} \quad (5)$$

In Equation (5) ΔR_{ax}^i and ΔR_{eq}^i represent the deviation of the axial and equatorial ammonia molecules from their equilibrium positions for the Mn^{III} and Mn^{IV} centers. The equilibrium position corresponds to $q_N = 0$ Å and the symmetrical geometry to $|q_N| = 0.073$ Å. Calculations were performed for different values of q_O defined as the displacement in Å of the oxygen atoms from the equilibrium position along the x axis. The computed points are shown in a pseudo-three-dimensional representation in Figure 4. A rather flat saddle

0947-6539/02/0821-5024 $ 20.00+.50/0 Chem. Eur. J. 2002, 8, No. 21

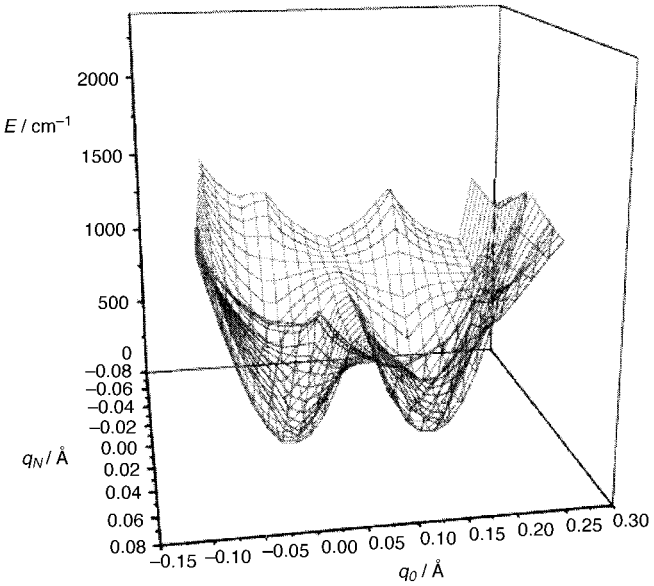

Figure 4. Pseudo-three-dimensional representation of the potential energy surface computed for $[Mn_2O_2(NH_3)_8]^{3+}$. The q_N and q_0 coordinates are defined in the text.

surface is computed for $q_O = 0.07$ Å, which corresponds to the symmetric oxygen bridge between the two manganese ions: this shows that the motion of the nitrogen atoms alone is not efficient enough to localize the "extra" electron.

The above analysis was performed on the high-spin states. These are actually excited states of the systems since the calculation of the magnetic coupling provides an overall antiferromagnetic interaction in both Mn^{II}/Mn^{III} and Mn^{III}/Mn^{IV} complexes. To extend the above results to the lower spin states independent calculations should be performed for each spin state. This procedure cannot be followed within density functional theory, since the lower spin states do not have a single determinant representation. Therefore, we follow the model developed by Girerd et al., which is based on a spin Hamiltonian approach.[8, 9] Within this formalism, the energies of the spin states are obtained by diagonalizing the 2×2 potential energy matrix, $\tilde{M}$, between two localized states of spin S, namely $|S_A^* S_B S M_s\rangle$ and $|S_A S_B^* S M_s\rangle$, A and B labeling the center on which the unpaired electron is localized.

$$\tilde{M} = \begin{array}{c|cc} & |S_A^* S_B S M_s\rangle & |S_A S_B^* S M_s\rangle \\ \hline \langle S_A^* S_B S M_s| & \frac{JS(S+1)}{2} + lQ + \frac{kQ^2}{2} - \frac{gQ^3}{6} & \frac{\beta(2S+1)}{2(2S_0+1)} \\ \langle S_A S_B^* S M_s| & \frac{\beta(2S+1)}{2(2S_0+1)} & \frac{JS(S+1)}{2} - lQ + \frac{kQ^2}{2} + \frac{gQ^3}{6} \end{array}$$

Here we have added the anharmonic cubic term g, to the vibrational potential, β is the electron transfer integral between the A and B centers, and S_0 is the spin of the center without the "extra" electron.

By diagonalization of $\tilde{M}$ two energies are obtained. The energies computed with $g = 0$ for a generic spin state S are graphically shown in Figure 5, where relevant points on the potential curve are shown and labeled according to standard

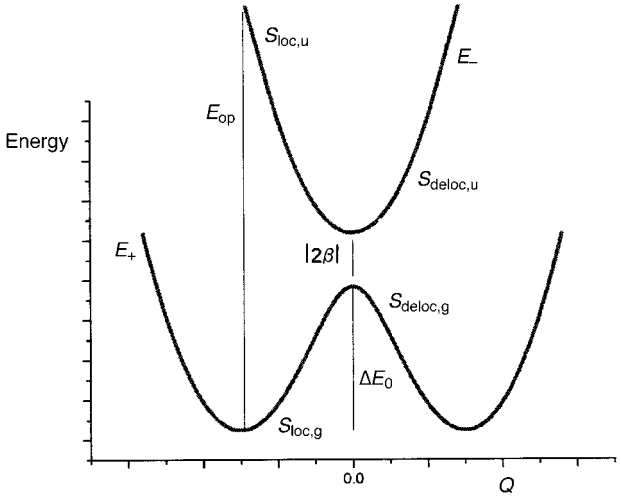

Figure 5. General soltion of the Hamiltonian matrix (Equation (5)) labeling the relevant points of the energy curve.

conventions. The β parameter appearing in $\tilde{M}$ for the Mn^{II}/Mn^{III} and Mn^{III}/Mn^{IV} systems can be computed from the high-spin states (HS) by using Equation 6[8, 9] by computing the excitation of the "extra" electron between the symmetric and antisymmetric linear combinations of d_{xy} and d_{z^2}, for the Mn^{II}/Mn^{III} and Mn^{III}/Mn^{IV} cases respectively.

$$2\beta = E(\mathrm{HS_{deloc,u}}) - E(\mathrm{HS_{deloc,g}}) \quad (6)$$

With these calculations we obtained $\beta = 1045\ \mathrm{cm^{-1}}$ and $696\ \mathrm{cm^{-1}}$, respectively.

The E_{op} transition, usually referred to as the metal-to-metal charge transfer, was computed on the more stable geometry using the Slater transition state[42] procedure at $14300\ \mathrm{cm^{-1}}$ and $13800\ \mathrm{cm^{-1}}$ for the Mn^{II}/Mn^{III} and Mn^{III}/Mn^{IV} systems respectively. The latter figures compare nicely with the transition around $12000\ \mathrm{cm^{-1}}$ experimentally observed in a number of compounds.[43]

Using the lowest energy root of $\tilde{M}$ the points on the curves of Figure 3 can be fitted by a least-squares procedure keeping β fixed at the values previously computed, and using J, k, l, and g as free parameters. The results of the fit are shown in Table 5, were also the computed β and E_{op} values are reported. When using matrix $\tilde{M}$ to fit the data of Figure 3, the exchange-coupling constant J assumes the role of a scale factor, since the zero of the energy in Figure 3 is the minimum

Table 5. Vibronic parameters, transfer integrals E_{op} and E_0 computed for the $[Mn^{(N)}{}_2O_2(NH_3)_8]^{n+}$ ($n = 1, 3$; N = II/III, III/IV) cations.[a]

n	l [$\mathrm{cm^{-1}\,bohr^{-1}}$]	k [$\mathrm{cm^{-1}\,bohr^{-2}}$]	g [$\mathrm{cm^{-1}\,bohr^{-3}}$]	β [$\mathrm{cm^{-1}}$]	E_{op} [$\mathrm{cm^{-1}}$]	E_0 [$\mathrm{cm^{-1}}$]
1	805(12)	179(9)	1.3(1)	1045	14300	660
3	3272(45)	3082(25)	17.7(1)	696	13800	875

[a] Standard deviations are reported in parenthesis.

  0947-6539/02/0821-5025 $ 20.00+.50/0

of the potential curve. We point out that from the results of the calculation of the PEC, it can be anticipated that matrix $\tilde{M}$ cannot be a good description for the Mn^{III}/Mn^{IV} system, since the oscillators on the two metal centers seem to be significantly coupled and a more general approach would be required. The harmonic frequency computed for this system ($\omega_{loc} = 627\ cm^{-1}$) is comparable to that obtained from the PES study ($\omega = 459\ cm^{-1}$). For the Mn^{II}/Mn^{III} case, for which the model of the uncoupled oscillators seems more appropriate, the computed frequency is $\omega_{loc} = 147\ cm^{-1}$. This value can be related[44] to that obtained from the PES analysis ($\omega = 218\ cm^{-1}$), using the model of two localized oscillators of unitary mass: in that case, $\omega = \sqrt{2}\omega_{loc}$, which yields $\omega = 207\ cm^{-1}$.

Using the data of Table 5 it is possible to compute the ratio λ/β, $\lambda = l^2/\kappa$ for the two mixed-valence species as 3.5 and 3.3 for Mn^{II}/Mn^{III} and Mn^{III}/Mn^{IV}, respectively. This value is in agreement with the assignment of both systems to Class II mixed-valence compounds.[45] The calculation of J was, therefore, performed by using the broken symmetry formalism (Equation (4)) on the geometry of minimum energy. The computed J values were $200\ cm^{-1}$ and $651\ cm^{-1}$ for Mn^{II}/Mn^{III} and Mn^{III}/Mn^{IV}, respectively. The experimental values for the Mn^{III}/Mn^{IV} compounds are close to $300\ cm^{-1}$, in qualitative agreement with the computed value, as already obtained for the integer valence systems. The computed exchange-coupling constants are antiferromagnetic in both cases. Following the same qualitative description of the exchange pathways used for the integer valence systems, we computed the square of the overlap integrals, which are reported in Table 6. The overlap integrals decrease on passing from the Mn^{III}/Mn^{IV} to the Mn^{II}/Mn^{III} systems, probably as a consequence of the increase in the bridging Mn-O-Mn angle. In the Mn^{III}/Mn^{IV} case the overall decrease of the overlap integrals is balanced by the large overlap between $d_{x^2-y^2}$ and d_{z^2} (0.1935) and the computed J value is close to that of the Mn^{IV}/Mn^{IV} case.

Using the computed J and β values in matrix $\tilde{M}$ and the values of l, k, and g from Table 5, the energies of the spin states shown in Figure 6 are obtained. As expected, ΔE_0 increases on going to the lower symmetry states, and the localization of the electron increases consequently.

Table 6. Squared overlap integrals between the magnetic orbitals for the $[Mn^{(N)}{}_2O_2(NH_3)_8]^{n+}$ ($n = 1, 3$; N = II/III, III/IV) cations.[a]

n	$\langle b_2 \mid b_2\rangle^2$	$\langle a_2 \mid a_2\rangle^2$	$\langle a_1 \mid a_1\rangle^2$	$\langle a_1(z^2) \mid a_1(z^2)\rangle^2$	$\langle b_1 \mid b_1\rangle^2$	$\langle a_1 \mid a_1(z^2)\rangle^2$
1	0.00	0.044	0.038	0.006	–	0.046,0.041[b]
3	0.055	0.001	0.066	–	–	0.19

[a] The magnetic orbitals are labeled according to the C_{2v} symmetry group (see text). [b] The two values refer to the overlap $\langle a_1\alpha \mid a_1(z^2)\beta\rangle^2$ and $\langle a_1\beta \mid a_1(z^2)\alpha\rangle^2$, respectively.

Conclusion

A complete characterization of the magnetic interactions in di-manganese systems of general formula $[MnO(L_4)]_2$ (L_4 = nitrogen ligand) has been performed using DFT and effective vibrational methods. The variation of the squared overlap integrals between the magnetic orbitals was used to ration-

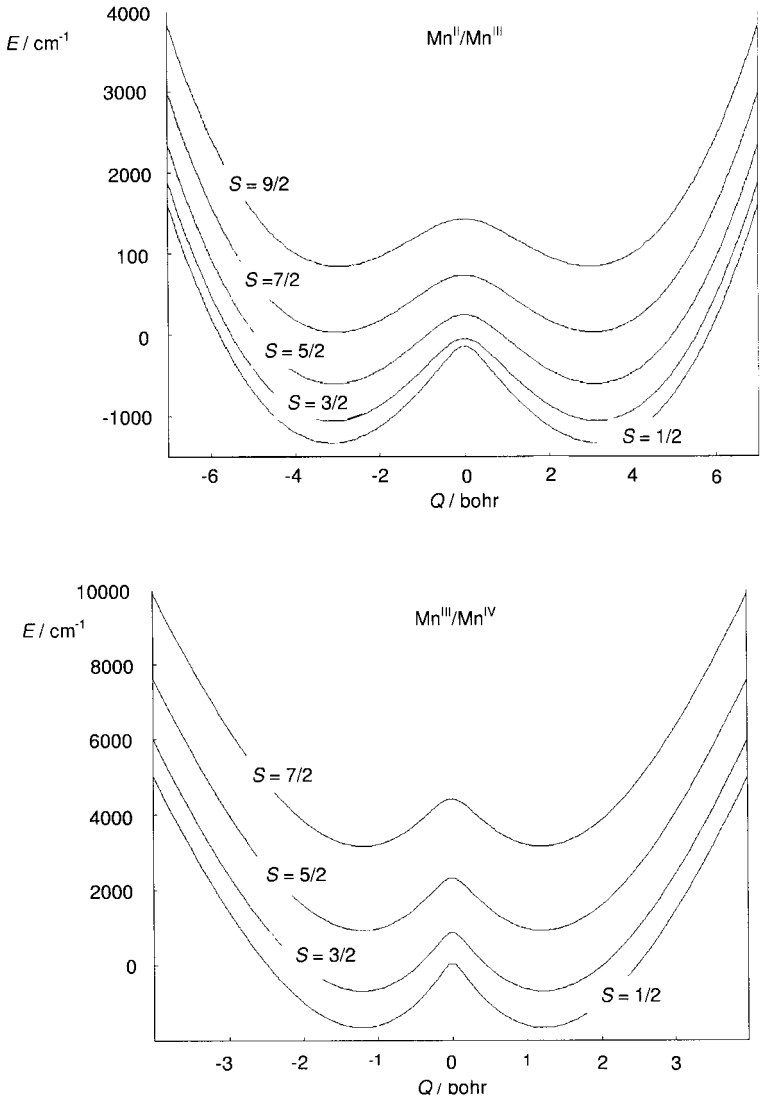

Figure 6. Dependence of the energies of the different spin states for $[Mn_2O_2(NH_3)_8]^+$ (top) and $[Mn_2O_2(NH_3)_8]^{3+}$ (bottom) on the nuclear displacement Q.

0947-6539/02/0821-5026 $ 20.00+.50/0 *Chem. Eur. J.* **2002**, *8*, No. 21

alize the trend of J values computed on passing from the Mn^{II}/Mn^{II} to Mn^{IV}/Mn^{IV} systems. The magnetic orbitals were directly obtained from the eigenvectors of the broken symmetry state. Our effective vibrational method was found helpful for analyzing the potential energy surface of the mixed-valence complexes. This allows one to estimate B and the delocalized nature of the compound and it can be of help in the experimental characterization of the magnetic properties of mixed-valence systems.

Acknowledgements

Thanks are expressed to Fabio Mariotti, University of Fribourg (Switwerland), who performed the calculation of S^2 from the eigenfunctions of ADF. A special thank is addressed to Alessandro Ferretti, CNR of Pisa (Italy) for the helpful discussions and suggestions. This work was supported by MIUR under the national project "Molecular nanotechnologies for magnetic and non-linear optical materials" 2001, by EC network MOLNANOMAG (contract no HPRN-CT-1999-00012), CNR PF MSTA II, INFM P.R.A.

[1] J. B. Goodenough, *Progr. Solid State Chem.* **1971**, *5*, 145.
[2] a) C. N. R. Rao, A. K. Cheetham, R. Mahesh, *Chem. Mater.* **1996**, *8*, 2421; b) B. Raveau, A. Maignan, C. Martin, M. Hervieu, *Chem. Mater.* **1998**, *10*, 2641.
[3] E. Coronado, C. J. Gomez-Garcia, *Comments Inorg. Chem.* **1995**, *17*, 255.
[4] E. L. Bominaar, S. A. Borsch, J. J. Girerd, *J. Am. Chem. Soc.* **1994**, *116*, 5362.
[5] E. L. Bominaar, Z. Hu, Münck, J. J. Girerd, S. A. Borsch, *J. Am. Chem. Soc.* **1995**, *117*, 6976.
[6] C. Zener, *Phys. Rev.* **1951**, *82*, 403.
[7] P. W. Anderson, H. Hasegawa, *Phys. Rev.* **1955**, *100*, 675.
[8] G. Blondin, J. J. Girerd, *Chem. Rev.* **1990**, *90*, 1359.
[9] O. Kahn, *Molecular Magnetism*, VCH Publishers, New York, **1993**.
[10] J. J. Borrás-Almenar, E. Coronado, A. V. Palii, B. S. Tsukerblat, R. Georges, *Chem. Phys.* **1998**, *226*, 231.
[11] J. J. Borrás-Almenar, J. M. Clemente, E. Coronado, A. V. Palii, B. S. Tsukerblat, R. Georges, *J. Chem. Phys.* **1996**, *105*, 6892.
[12] M. B. Robin, P. Day, *Adv. Inorg. Chem. Radiochem.* **1967**, *10*, 247.
[13] A. Bencini, I. Ciofini, C. Daul, A. Ferretti, *J. Am. Chem. Soc.* **1999**, *121*, 11418.
[14] V. Barone, A. Bencini, I. Ciofini, C. A. Daul, F. Totti, *J. Am. Chem. Soc.* **1998**, *120*, 8357.
[15] K.-O. Schäfer, R. Bittl, W. Zweygart, F. Lendzian, G. Haselhorst, T. Weyhermüller, K. Wieghardt, W. Lubitz, *J. Am. Chem. Soc.* **1998**, *120,* 13104.
[16] a) P. A. Goodson, A. R. Oki, J. Glerup, D. J. Hodgson, *J. Am. Chem. Soc.* **1990**, *112*, 6248; b) P. A. Goodson, J. Glerup, D. J. Hodgson, K. Michelsen, E. Pedersen, *Inorg. Chem.* **1990**, *29*, 503; c) M. Stebler; A. Ludi, H.-B. Bürgi, *Inorg. Chem.* **1986**, *25*, 4743; d) A. R. Oki, J. Glerup, D. J. Hodgson, *Inorg. Chem.* **1990**, *29*, 2435; e) M. A. Collins, D. J. Hodgson, K. Michelsen, D. K. Towle, *J. Chem. Soc. Chem. Commun.* **1987**, 1659; f) K. S. Hagen, W. H. Armstrong, H. Hope, *Inorg. Chem.* **1988**, *27*, 969; g) S. R. Cooper, G. C. Dismukes, M. P. Klein, M. Calvin, *J. Am. Chem. Soc.* **1978**, *100*, 7248; h) S. R. Cooper, M. Calvin, *J. Am. Chem. Soc.* **1977**, *99*, 6623; i) P. M. Plaksin, R. C. Stoufer, M. Mathew, G. J. Palenik, *J. Am. Chem. Soc.* **1972**, *94*, 2121; l) M. Suzuki, S. Tokura, M. Sihara, A. Uehara, *Chem. Lett.* **1988**, 477; m) D. K. Towle, C. A. Botsford, D. J. Hodgson, *Inorg. Chim. Acta* **1988**, *141*, 167; n) K. J. Brewer, M. Calvin, R. S. Lumpkin, J. W. Otvos, L. O. Spreer, *Inorg. Chem.* **1989**, *28*, 4446; o) P. A. Goodson, J. Glerup; D. J. Hodgson; K. Michelsen, *Inorg. Chim. Acta* **1990**, *172*, 49; p) S. Schindler, O. Walter, J. Z. Pedersen, H. Toftlund, *Inorg. Chim. Acta* **1999**, *303*, 215; q) J. Glerup, P. A. Goodson, A. Hazell, R. Hazell, D. J. Hodgson, C. J. McKenzie, Michelsen, K. U. Rychlewska, H. Toftlund, *Inorg Chem.* **1994**, *33*, 4105.
[17] a) G. C. Dismukes, *Chem. Rev.* **1996**, *96*, 2909; b) V. L. Pecoraro, *Manganese Redox Enzymes*, VCH Publishers, Weinheim, **1992**; c) V. K. Yachandra, K. Sauer, M. P. Klein, *Chem. Rev.* **1996**, *96*, 2927.
[18] K.-F. Hsu, S.-L. Wang, *Chem. Commun.* **2000**, 135.
[19] X. G. Zhao, W. H. Richardson, J.-L. Chen, L. Noodleman, H.-L. Tsai, D. N. Hendrickson, *Inorg. Chem.* **1997**, *36*,1198.
[20] J. E. McGrady, R. Stranger, *J. Am. Chem. Soc.* **1997**, *119*, 8512.
[21] P. A. Goodson, D. J. Hodgson, *Inorg. Chim. Acta*, **1990**, *172*, 49, and references therein.
[22] C. Adamo, V. Barone, A. Bencini, F. Totti, I. Ciofini, *Inorg. Chem.* **1999**, *38*, 1996.
[23] A. D. Becke, *J. Chem. Phys.* **1993**, *98*, 5648.
[24] a) H. Chevreau, I. de R. R. Moreira, B. Silvi, F. Illas, *J. Phys. Chem. A* **2001**, *105*, 3570; b) E. Ruiz, J. Cano, S. Alvarez, P. Alemany *J. Comp. Chem.* **1999**, *20*, 1391; c) "Magnetism: Molecules to Materials II", (Eds.: J. S. Miller, M. Drillon), VCH-Wiley, **2001**, chapter 7; d) E. Ruiz, P. Alemany, Alvarez, S. Alvarez, J. Cano, *Inorg. Chem.* **1997**, *36*, 3683.
[25] ADF 2.2, ADF 2.3, Theoretical Chemistry, Vrije Universiteit, Amsterdam.
[26] a) E. J. Baerends, D. E. Ellis, P. Ros, *Chem. Phys.* **1973**, *2*, 41; b) G. te Velde, E. J. Baerends, *J. Comput. Phys.***1992**, *99*, 84.
[27] J. C. Slater, *Quantum Theory of Molecules and Solids, Vol. 4, Self-Consistent Field for Molecules and Solids*, McGraw-Hill, New York, **1974**.
[28] S. H. Vosko, L. Wilk, M. Nusair, *Canadian J. Phys.* **1980**, *58*, 1200.
[29] H. Stoll, C. M. E. Pavlidou, H. Preuss, *Theor. Chim. Acta* **1978**, *49*, 143.
[30] a) V. Barone in *Recent Advances in Density Functional Methods*, *vol. 1* (Ed.: D. P. Chang), World Scientific, Singapore, p. 287, **1996**; b) DiNa Program, Release 2.1, by V. Barone, University of Naples.
[31] I. Ciofini, C. A. Daul, A. Bencini in *Recent Advances in Density Functional Methods*, *vol.3* (Eds. V. Barone, A. Bencini, P. Fantucci), World Scientific, Singapore, in press.
[32] a) L. Noodleman, J. G. Jr. Norman, *J. Chem. Phys.* **1979**, *70*, 4903. b) L. Noodleman, *J. Chem. Phys.* **1981**, *74*, 5737; c) L. Noodleman, D. A. Case, S. F. Sontum, *J. Chim. Phys.* **1989**, *86*, 743. d) A. Bencini, *J. Chim. Phys.* **1989**, *86*, 763; e) L. Noodleman, C. Y. Peng, D. A. Case, J. M. Mouesca, *Coord. Chem. Rev.* **1995**, *144*, 199.
[33] R. Caballol, O. Castell, F. Illas, I. P. R. Moreira, J. P. Malrieu, *J. Phys. Chem.* **1997**, *101*, 7860.
[34] T. Soda, Y. Kitagawa, T. Onishi, Y. Takano, Y. Shigeta, H. Nagao, Y Yoshioka, K. Yamaguchi, *Chem. Phys. Letters* **2000**, *319*, 223.
[35] a) A. D. Becke, *J. Chem. Phys.* **1986**, *84*, 4524; b) J. P. Perdew, *Phys. Rev. B* **1986**, *33*, 8822
[36] A. Bencini, F. Totti, C. A. Daul, K. Doclo, P. Fantucci, V. Barone, *Inorg. Chem*. **1997**, *36*, 5022.
[37] a) E. Ruiz, P. Alemany, S. Alvarez, J. Cano, *J. Am. Chem. Soc.* **1997**, *119*, 1297; b) E. Ruiz, J. Cano, S. Alvarez, P. Alemany, *J. Am. Chem. Soc.* **1998**, *120*, 11122.
[38] a) P. De Loth, P. Cassoux, J. P. Daudey, J. P. Malrieu, *J. Am. Chem. Soc.* **1981**, *103*, 4007; b) P. De Loth, J. P. Daudey, J. P. Malrieu in *Magneto Structural Correlations in Exchange Coupled Systems*, (Eds.: D. Gatteschi, O. Kahn, D. Willett), *vol. 140*, NATO Advanced Studies Ser. C, Reidel, Dordrecht, **1985**; c) J. Miralles, J. P. Daudey, R. Caballol, *Chem. Phys. Lett.* **1992**, *198*, 555; d) J. Miralles, O. Castell, R. Caballol, J. P. Malrieu, *Chem. Phys.* **1993**, *172*, 33; e) J. Miralles, O. Castell, R. Caballol, *Chem. Phys.* **1994**, *179*, 377.
[39] P. Bertrand, *Inorg. Chem.* **1993**, *32*, 741.
[40] V. Barone, C. Adamo, *Chem. Phys. Lett.* **1995**, *241*, 1.
[41] V. Barone, C. Minichino, *Theochem* **1995**, *330*, 325.
[42] J. C. Slater, *The Self-consistent Field for Molecules and Solids: Quantum Theory of Molecules and Solids, Vol. 4, International Series in Pure and Applied Physics*, (Eds.: J. L. Farnsworth, C. First), McGraw-Hill, **1974**.
[43] a) S. R. Cooper, G. C. Dismukes, M. P. Klein, M. Calvin, *J. Am. Chem. Soc.* **1978**, *100*, 7248; b) S. R. Cooper, M. Calvin, *J. Am. Chem. Soc.* **1977**, *99*, 6623.
[44] a) G. Herzberg, *Infrared and Raman Spectra of Polyatomic Molecules*, Van Nostrand, Toronto, **1945**, 172; b) J. I. Steinfield, *Molecules and Radiation*, Harper & Row, New York, **1974**, 181.
[45] V. Papaefthymiou, J. J. Girerd, I. Moura, J. J. G. Moura, E. Münk, *J. Am. Chem. Soc.* **1987**, *109*, 4703.

Received: February 18, 2002 [F3884]

  0947-6539/02/0821-5027 $ 20.00+.50/0